Light Metals 2014
Edited by: John Grandfield
TMS (The Minerals, Metals & Materials Society), 2014

TENSILE AND SHEAR MECHANICAL PROPERTIES IN A THERMO-MECHANICAL-ELECTRICAL PROCESSED SPOT WELD

S.A. Turnage[1], K.N. Solanki[1*], W.R. Whittington[2], R.S. Florea[2], M.A. Tschopp[3], K.A. Darling[3]
[1]School for Engineering of Matter, Transport, and Energy, Arizona State University, Tempe, AZ 85287;
[2]Center for Advanced Vehicular Systems, Mississippi State University, 200 Research Blvd., Starkville, MS 39759
[3]Army Research Laboratory, Weapons and Materials Research Directorate, APG, MD 21014
*Corresponding Author: E-mail: kiran.solanki@asu.edu

Keywords: Resistance Spot Weld, Al 6061-T6, Mechanical Properties, Shear Punch

Abstract

This study offers a novel approach to characterize the microstructure-property relationship of RSW Al6061-T6 aluminum alloy lap joints. Here, the mechanical properties are determined from quasi-static tensile tests along with shear punch tests through the weld regions. Using measured shear and tensile data, a linear correlation is obtained to quantify the yield and ultimate strengths across the weld region. Furthermore, shear punch tests were also performed in the rolling, transverse, and normal directions of the weld and rolled plate to quantify material anisotropy due to underlying solidification induced microstructure. Future work will explore how the observed mechanical responses are correlated with changes in the microstructures using neutron diffraction and stereological techniques.

Introduction

The automotive and defense industries require welding in lightweight alloys to decrease the weight of ground vehicles, thereby addressing energy and emission concerns, improving fuel economy, and reducing production costs. Accomplishing this is no small task, as it requires new lightweight structural alloys and *joining techniques* that can efficiently form these metals into components. In fact, it is the limitations of existing joining techniques that currently hinders widespread use of lightweight alloys; for example, use of ultra-high strength steel is not often utilized because of the brittle weld microstructures produced by traditional resistant spot welding (RSW) [1,2]. These welding operations often involve intense thermal gradients and melt convection that results in a continually evolving microstructure away from that of the base material. Particularly in RSW, an intense melt flow is caused by the induced electromagnetic field. Due to this, a non-homogeneous distribution of the material microstructure often exists. These residual microstructures, present in crystalline materials after processing, influence the overall strength and performance of the joints. As such, quantifying the influence of process-induced microstructural changes and subsequent effects on mechanical properties are technologically important in advanced energy, transportation, and manufacturing industries.

Thermo-mechanical-electrical joining processes, such as RSW, have deleterious effects on the strength and failure behavior of metal components which is an issue that still perplexes material scientists and mechanical engineers. In fact, experimental and computational modeling of the RSW processes to study the effect of weld process parameters on joint strength and failure has received much attention in the last several decades [2-29]. Bowden and Williamson were the first to investigate interface behavior between two contact solids and showed that the surface asperities condensed current density and restricted contact resistance within the contact region, which caused temperature to rise at the interface when electric current flow occurred [8]. A detailed theoretical and experimental study by Bentley and Greenwood [12] showed that the contact resistance played a major role only in the very early stages of heat generation and became less influential in the later stages of the weld nugget formation. Using the one-dimensional heat models of Bowden and Williamson [8] and Greenwood [9], Gould [11] studied the RSW process by including the electrode geometry, internal heat generation, phase change, temperature-dependent material properties and contact resistance. Through this, Gould [11] showed that the predicted nugget sizes were much larger than those observed in the experiment and concluded that this discrepancy was evidently due to neglecting the radial heat loss to the surrounding sheet. More recently, Nied [10], Sheppard [14], Tsai et al. [15-16], Browne et al. [17-18], Dong et al. [20], Khan et al. [22-23], Sun and Dong [24], and Murakawa et al. [19] all performed theoretical and experimental studies to address different aspects of the RSW process, including nugget formation, electrode design and electrode wear. Nishu and Murakawa [25] experimentally and numerically investigated the nugget formation process purely based on nugget size; they concluded minimum weld-ability conditions are required for a RSW of high strength stainless steel sheets. Hamedi and Pashazadeh [26], using a very phenomenological model, studied the effect of weld process parameters on nugget formations and concluded that, at low electrode forces and high welding currents, the formed fusion zone is large. Zhang and Senkara [4] and Williams and Parker [5] provided a detailed review of several experimental and theoretical studies which have previously investigated the mechanical and physical properties of RSW joints. Florea et al. [6] investigated the effect of weld current on RSW quality and found that depth of the weld nugget varies linearly with weld current. They also noted that weld current affected the microstructure and shear strength of the lap joint.

As illustrated in Figure 1a, the RSW process joins two metal sheets through compression between a pair of water-cooled electrodes with an external applied force. Low-voltage, high-amperage electric current passes through the sheets for a short duration via the two electrodes, generating concentrated heating at the contact surface. Due to both the heat generation at the contact surface and joule heating, a molten zone forms at the intersection of the two sheets. After the current flow ceases, the electrode force is maintained for another short duration to allow the work-piece to rapidly cool and solidify. The contact surface area depends on the electrode diameter, applied force, temperature, and metal deformation.

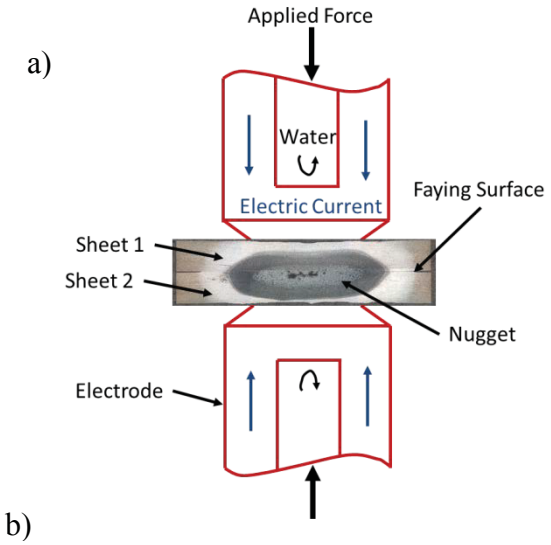

b)

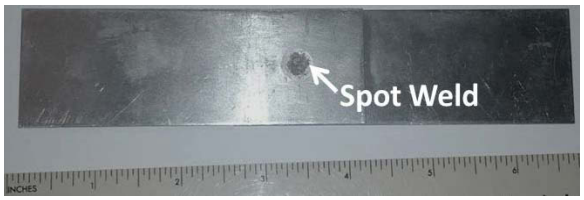

c)

Weld Parameters		
	Electrode force	3.8 kN
	Time	0.115 s
Current	Process #1	26 kA
	Process #2	30 kA
	Process #3	36 kA
	Voltage	8 VDC
	Water flow rate	4 liters/min

Figure 1. a) Schematic drawing of resistant spot welding (RSW); b) A RSW-produced Al6061-T651 lap joint; and c) weld parameters.

In this study, we use a novel approach to characterize the mechanical properties, which will later be utilized to develop a structure-property database of RSW 6061-T6 aluminum lap joints for use in finite element analyses. More specifically, the mechanical properties are determined from quasi-static tensile tests along with quasi-static shear punch tests through the weld regions. Using measured shear and tensile data, a linear correlation is obtained to quantify the yield and ultimate strengths across the weld region. Future work will explore how the observed mechanical responses are correlated with changes in the microstructures using neutron diffraction and stereological techniques.

Experimental Procedures

For this study, a servo-gun, with weld control and copper-zirconium alloy electrodes, was used to manufacture the specimens from a sheet of 6061-T6 aluminum. The aluminum

a)

b)

	Base Material	Spot Weld
Gage Length [mm]	4.77	4.72
Gage Width [mm]	2.01	2.03
Thickness Quasistatic [mm]	1.95	2.14

c)

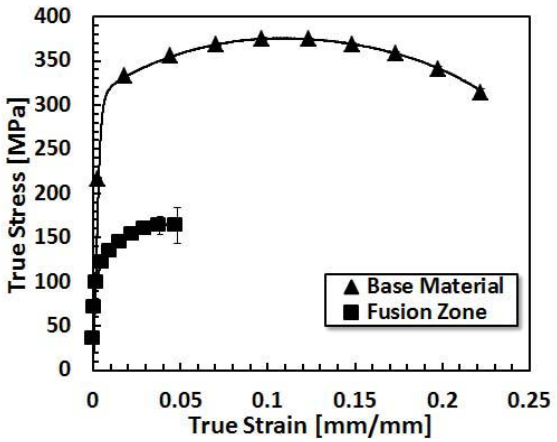

Figure 2. a) Miniature dog-bone specimens were extracted from the weld region and from the base material, b) overall dimensions of dog-bone specimens, and c) Quasi-static strain rate tensile stress-strain curve in the fusion zone shows, in contrast to the base material, a significant reduction in tensile strength and ductility.

sheets were approximately 5 inch length by 1.5 inch width by 2 mm thick. The power supply and current transformer had a mid-frequency direct current with 8 V on the secondary voltage. Water was applied as a cooling agent at a rate of 4 liters/minute. For further detail about the weld sample preparation please refer to [6]. Electrode force (3.8 kN), weld time (0.115 s) and weld current (30 kA) (see [6]) were manually optimized to produce a minimum nugget size of 5.7 mm with minimum shearing force of 3.8 kN per weld. The optimized welds meet or exceed the MIL-W-6858D Military specification [27]. The weld process and weld parameters are outlined in Figure 1.

Small, flat, dog-bone shaped specimens were cut from the center of the weld sheets as well as from the parent material using a wire electrical discharge machine for the quasi-static tensile testing. Specimens were cut with gauge length along the rolling direction of the aluminum sheet. Dog-bone specimens and general dimensions can be seen in Figure 2a-b. Quasi-static tensile tests were performed at a strain rate of 0.001 /s on an electromechanically driven monotonic tensile tester. No fewer than two tests were run for the weld region and the parent material. Figure 2c shows tensile stress-strain curves produced using miniature dog-bone specimens taken from the weld section and the base material. The stress-strain curves reveal a significant reduction in tensile strength and ductility for the weld section.

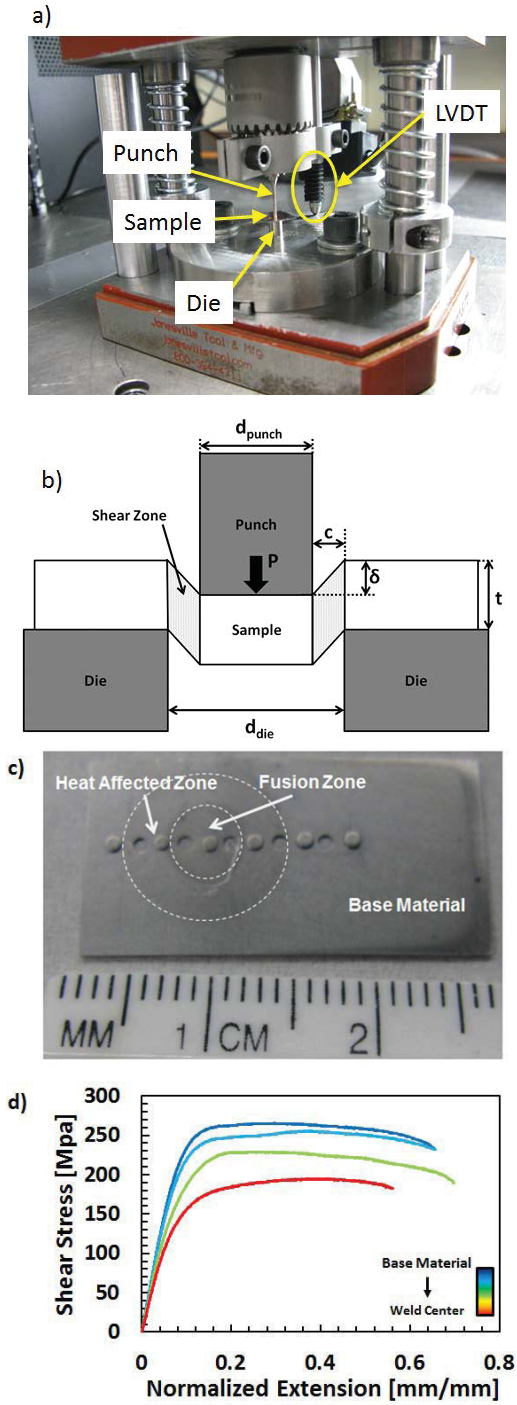

Figure 3. a) Shear punch setup, b) schematic of shear punch test, c) location of shear punch testing with respect to weld zone, and d) the shear stress evolution as a function of normalized extension for different sections of the weld as highlighted in c). Comparing the mechanical behavior at different sections of the weld shows a profound effect of the solidification induced microstructure.

Shear punch testing utilizing a punch diameter of approximately 1 mm with punch-die clearance of approximately 30 µm was performed through the weld in the rolling, transverse, and normal directions of the original rolled plates. As can be seen

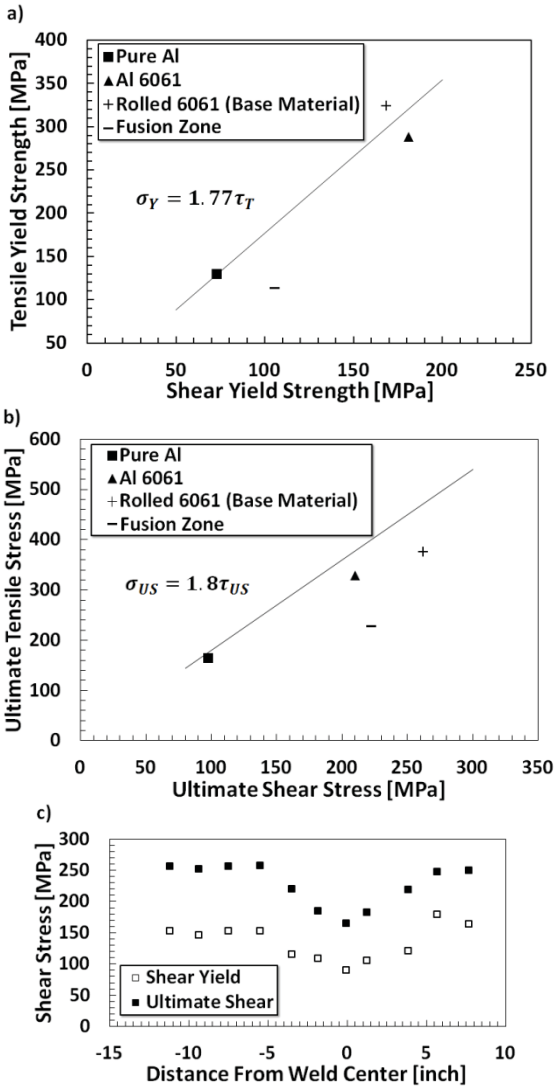

Figure 4. Correlation of mechanical testing results with a) von Mises and b) Tresca criteria. c) Shear yield and ultimate shear strength at points spaced approximately 1.5 mm through the weld region.

in Figure 3, the shear punch drives the solid cylindrical punch through a thin plate specimen into a hollow cylindrical die. Here, the displacement is normalized by the specimen thickness providing a consistent comparison between the test results [30]. The shear stress evolution as a function of normalized extension for the different sections in the welded region is shown in Figure 3d. The comparison of the mechanical behavior at different sections of the weld region shows profound effect of solidification induced microstructure.

Results and Discussions

Figure 2b shows tensile stress-strain curves produced using miniature dog-bone specimens taken from the weld section and the base material. The stress-strain curves reveal a significant reduction in tensile strength and ductility for the weld section. The rolled 6061-T6 aluminum alloy base material has yield strength of

290 MPa and an ultimate strength of 375 MPa. In contrast, the welded portion of the material has yield strength of 95 MPa and ultimate strength of 165 MPa, i.e., ~33% and 44% lower yield and ultimate strengths, respectively, when compared with the base material. This illustrates the weakening effects of the intense temperature gradient and compressive strain from the welding process on the mechanical properties of 6061-T6 aluminum alloy. While RSW bonds are frequently strong, they most commonly fail in the heat affected zone (HAZ), which is due to a lack of ductility created as the HAZ becomes brittle during the welding process. In turn, it is possible to predict the degree of embrittlement through estimation of the change in strength using SPT technique. Figure 3d shows the shear stress evolution, measured using SPT, as a function of normalized extension for the different sections in the welded region as highlighted in Figure 3c. From the shear punch data, as shown in Figure 3d, the 1% offset criterion could be used to calculate the shear yield stress and also the shear ultimate (maximum) stress. Figures 4a and 4b shows the correlation of measured shear properties with the tensile properties for the base and fusion zone which satisfies the relation $\sigma_{ys} = 1.77\tau_{ys}$ and $\sigma_{us} = 1.8\tau_{us}$ for the yield and ultimate strength, respectively. Here we used the pure aluminum and 6061 data for comparison from Guduru et al. [30]. The evolution of shear properties measured through the weld region are also shown in Figure 4c, which reveals that material strength decreases in the HAZ and is at the lowest point, about 43% lower than the base material, near the center of the weld. The loss of T6 condition, which occurs during welding, is expected to decrease the mechanical strength reflected in the drop of shear properties. Hence, during the weld thermal cycle, the increasing degree of dissolution of the precipitates from the base material to the center of the weld nugget causes progressive loss of strength, resulting in the observed shear strength profile across the cross section of the weld (Fig. 4c). It follows, then, that the hardening in Al-Cu alloys is achieved when dislocation motion is impeded by lattice strain and as resistance to shearing of precipitates by dislocations leads to the formation of Orowan loops around precipitates. Precipitates with an iron and silicon composition averaged areas of 8.76 μm^2, and 0.196 μm^2 in the base material and fusion zone respectively.

Shear punch tests were also performed in the rolling, transverse, and normal directions of the weld and rolled plate to quantify material anisotropy due to underlying solidification induced microstructure. Figure 5 shows the shear stress evolution as a function of normalized extension for the rolling, transverse, and normal directions. Interestingly, Figure 5 shows a minimal dependence on the orientation of the test relative to the original rolling direction of the plate. The base material and HAZ show increased strength in the normal direction and decreased elongation in the rolling direction. In the fusion zone, anisotropy appears to play a larger role.

To explain the detrimental effects of spot welding on the material strength and ductility, both residual stress measurements via neutron diffraction and microstructural characterization of grain size, grain misorientations, and precipitate sizes are currently underway. Preliminary results reveal an increase in the anisotropy of grain texture and misorientation distributions as the weld center is approached. Additionally, a notable grain size difference takes place as a result of resistance spot welding.

Conclusions

The microstructure-property relationships of RSW Al6061-T6 aluminum alloy lap joints were characterized using tensile and shear punch tests coupled with optical and scanning electron microscopy. Quasi-static tensile and shear punch tests revealed constantly decreasing strength and ductility as the weld center line was approached. Also from shear punch testing, an increase in anisotropy was noted in the fusion zone. Optical microscopy revealed a sharp decrease in both precipitate and grain size from the base material to the fusion zone. EBSD indicated greater uniformity of grain orientations in the fusion zone.

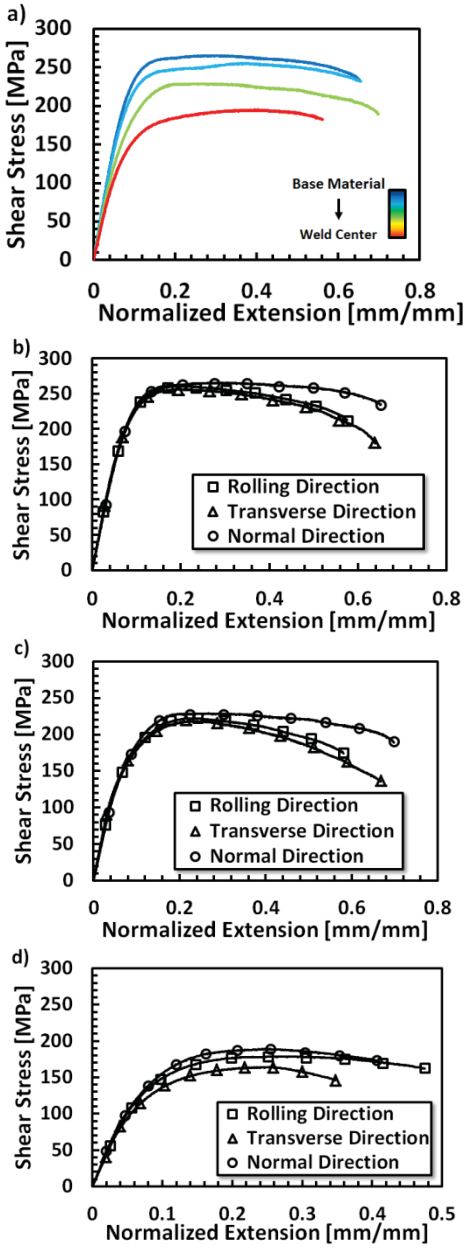

Figure 5. a) The shear stress evolution as a function of normalized extension for the different sections in the welded region. Mechanical response along the rolling, transverse, and normal directions for the b) base material, c) HAZ, and d) fusion zone. The fusion zone shows increased mechanical response dependence on direction.

References

1. J. Carpenter. AISI, "Automotive Lightweighting Materials" (Paper presented at the Great Designs in Steel Seminar, Livonia, MI, 2004), 96.
2. E. Del Vecchio. Resistance Welding Manual Third Edition: Volume 1, Resistance Welder Manufacturers' Association, (1956)
3. J. Sederstrom. "Spot friction welding of ultra-high-strength automotive sheet steel", (MS thesis, Brigham Young University, 2007).
4. N. Williams, J. Parker. "Review of resistance spot welding of steel sheets Part 1 Modelling and control of weld nugget formation", Int Mater Rev, 49 (2004) 45.
5. H. Zhang, J. Senkara. Resistance Welding: Fundamentals and Applications, CRC Press Taylor & Francis, London, 1 (2005).
6. R. Florea, K.N. Solanki, D. Bammann, J. Baird, J. Jordon, and M. Castanier. "Resistance spot welding of 6061-T6 aluminum: Failure loads and deformation" Mat. and Design, 34, (2011) 624-630.
7. W. Hess, W. Doty, W. Childs. "The Fundamentals of Spot Welding Steel Plate", Welding Journal, 610 (1947) 583.
8. F. Bowden, J. Williamson. "Electrical Conduction in Solids. I. Influence of the Passage of Current on the Contact between Solids", (Proceedings Royal Society, 1958), 1.
9. J. A. Greenwood, J. B. H. Williamson, Proceedings Royal Society, (1958) 13.
10. H. A. Nied, Welding Journal 63(4):123-132 (1984)
11. J. E. Gould, "An examination of Nugget development during spot welding using both experimental and analytical techniques", Welding Journal, 65(1): l-10 (1987)
12. H. S. Cho, Y. J. Cho, Welding Journal, 68(6): 236-244 (1989)
13. Z. Han, J. E. Orozco, C. H. Chen: Welding Journal, 67(9):363-371 (1989)
14. S. D. Sheppard: WRC Bulletin, 356: 34–41 (1990)
15. C. L. Tsai, W. L. Dai, D. W. Dicknson, J. C. Papritan: WRS, 70(12): 339–351 (1991)
16. C. L. Tsai, O. A. Jammal, C. Papritan, D. W. Dickinson: Welding Journal, 71(2): 47-54 (1992)
17. D. J. Browne, H. W. Chandler, J. T. Evans, J. Wen : Welding Journal, 74(10): 339-344 (1995)
18. D. J. Browne, H. W. Chandler, J. T. Evans, P. S. James, J. Wen, C. J. Newton: Welding Journal, 74(12): 417-422 (1995)
19. H. Murakawa, F. Kimura, Y. Ueda: In: Cerjak H (ed) Mathematical modeling of weld phenomena, The Institute of Materials, London, 944–966 (1997)
20. P. Dong, M. V. Li, M. Kimchi: Sci. and Tech. of Weld. and Join., 103–112 (1997)
21. O. P. Gupta, A. De: J. Manu. Sci. and Eng., Transaction of the ASME, 120: 246-251 (1998)
22. J. A. Khan, L. Xu, Y. J. Chao: Sci. and Tech. of Weld. and Join., 4: 201-207 (1999)
23. J. A. Khan, L. J. Xu, Y. J. Chao, K. Broach:, Num. Heat Trans., Part A, 37: 425–446 (2000)
24. X. Sun, P. Dong: Welding Research Supplement, 215-221 (2000)
25. M. A. Ninshu, H. Murakawa: Tran. of JWRL, 38(2): 19-24 (2009)
26. M. Hamedi, H. Pashazadeh. Inter. J. of Mech., 2(1) (2008), p.11.
27. MIL-W-6858D. Welding, resistance: spot and seam- the Department of Defense, Military specification; (1978), P.4.
28. R. Florea, C.R. Hubbard, K.N. Solanki, D.J. Bamman, W.R. Whittington, and E.B. Marin. Journal of Materials Processing and Technology, 212(11): 2358-2370 (2012)
29. Florea, R.S., Bammann, D.J., Yeldell, A., Solanki, K.N., Hammi, Y. Materials and Design, 45: 456–465 (2013)
30. R. K. Guduru, K. A. Darling, R. Kishore, R. O. Scattergood, C. C. Koch, and K. L. Murty, Mat. Sci. and Eng. A 395 (2005) 307-314